Survival of the unfittest: Metabolic trade-offs expose unforeseen benefits of plasmid carriage

CARLOS REDING[1,2*]

[1]*Living Systems Institute, University of Exeter, Exeter EX4 4QD, UK.*
[2]*Department of Genetics, Stanford School of Medicine, Stanford University. Stanford, CA 94305, USA.*
[*]**Corresponding author:** `reding@stanford.edu`

Population genetics theory defines fitness as reproductive success: Mutants reproducing faster than their wild-type counterpart are favoured by selection. Otherwise, the mutations are lost. Here I show that *unfit* mutants can thrive when selection favours non-reproductive traits if they engage in a trade-off with fitness. I co-maintained two constructs of *Escherichia coli*, with and without a non-transmissible plasmid, for more than 80 generations in competition assays that favoured yield. Plasmid carriage prompted a known metabolic trade-off in the bacterium between growth rate per capita—*reproductive success*—and yield. Importantly the plasmid carries a tetracycline-resistance gene, *tet(36)*. By favouring yield, cells harbouring the plasmid preserved it without exposure to the antibiotic. Unsurprisingly, these cells outgrew their fitter plasmid-free competitor with trace low tetracycline concentrations. Fitness competition assays are widely used, but experimental validation of their underlying principle is rare. These assays are the 'gold-standard' in genetics, but my work suggests their reliability may be lower than previously thought.

I. Introduction

The notion of 'fitness' is fundamental to understanding whether mutations are beneficial or deleterious. Population genetics defines (*1*) *fitness* as a population's reproductive rate: $N(t) = N_0 e^{mt}$, where N_0 is the initial population size, $N(t)$ population size at time t, and m the Malthusian reproductive rate. This notion is textbook in genetics (*2*) and, surprisingly, remains unchanged since the 1930s (*3*). Widely used in evolutionary biology (*4, 5*), fitness also has practical implications. Bacterial mutants resistant to antibiotics incur fitness costs (*6*). Epidemiologists exploit this phenomenon to design drug deployment strategies that minimise resistance in hospitals (*7–10*). Thus, fitness competition assays between two genotypes—mutant *versus* wild-type reference—emerged as the gold standard (*11*) method to quantify whether mutations are beneficial, neutral or deleterious. Whether the organism studied is unicellular (*11, 12*) or not (*13, 14*). But data is still lacking to validate many of the assumptions of population genetics theory (*15*).

Here I show that *unfit* mutants can thrive when fitness engages in a trade-off with biomass yield, consistently with *rK selection theory* (*16*). Contrary to population genetics, rK selection predicates that selection acts on populations in a manner that is contingent on their size and resource abundance (*16, 17*): Favouring mutations that increase fitness (r) in small populations with plenty of resources; and mutations that increase size in populations near their equilibrium (K)—larger and with fewer resources. Therefore, to test whether fitness is as good at predicting selection as claimed by population genetics, I applied rK selection theory and set up an unorthodox competition assay that favoured population size over fitness. The competing genotypes were a tetracycline-resistant construct of *Escherichia coli*, R, provided by a non-transmissible plasmid, and its sensitive counterpart S. The plasmid reduced the fitness of R-cells, however, it triggered a known

metabolic trade-off between fitness and biomass yield (*18*). In other words, R-cells divided at slower rates but attained larger population sizes.

Using this assay, I co-maintained both constructs for more than 80 generations without using tetracycline: R-cells did not perish despite their lower fitness. Importantly, during that time the number of plasmids borne by R-cells did not change substantially. Plasmids are often deemed costly because they hinder the host's fitness, however when fitness engages in a trade-off, here with yield, plasmids can provide unforeseen benefits.

II. Results

pGW155B hinders fitness of R-cells, but helps their yield. The expression of plasmid-borne genes is a metabolic burden that reduces the host's growth rate or *fitness* (*19–21*). Thus, to test whether fitness is a reliable metric for natural selection I designed a competition assay between two constructs of *Escherichia coli* MC4100 (*22*) (see Methods), one of which carries the non-transmissible plasmid pGW155B (*23*). This is a 5.4kb artificial plasmid that lacks the origin of transfer *oriT*, the relaxase to catalyse the initial and final stages in conjugation, type IV coupling protein (T4CP), and type IV secretion system (T4SS) required for either self-propagation or mobilisation by a trans-acting conjugative plasmid present in the same cell (*24*, and references therein) (addgene vector database accession #2853). The size of this plasmid is representative of those in nature (*25*) and, like many natural plasmids, pGW155B harbours antibiotic-resistance genes: *tet*(*36*), a ribosome-protection type resistance protein (*23*). The use of non-transmissible plasmids prevents cross-contamination during the competition assay between the resistant construct R, carrying the plasmid, and the reference, tetracycline-sensitive, S. Both constructs have identical chromosome with exception of the fluorescence gene they carry, cyan (*cfp*, R) or yellow (*yfp*, S), to allow their identification during the competition assay.

Growth data for each construct, grown as pure cultures and without tetracycline (Figure 1A), show that pGW155B penalised the growth rate of R-cells by 38.42% ± 12.39% (mean ± standard error with 8 replicates, Mann-Whitney U-test $p = 1.554 \times 10^{-4}$, ranksum = 100; Figure 1B) compared to their sensitive counterpart, S. Surprisingly, this data also showed noteworthy differences in two other growth parameters. First, R-cells—harbouring pGW155B—attained larger population sizes during the equilibrium compared to S. Regardless of whether I measured growth using fluorescence (Figure 1A) and optical density (Figure S1). Note that changes in cell size may confound optical density and fluorescence readings. This phenomenon, however, leaves a signature (*26*) in growth curve data that I did not find in my data (Figures S2, S1, S3 and S4). Now, crucially, this trait can be used to calculate biomass yield (y) as $y = K/glc$ (*18*, *27*), where K denotes population size at the equilibrium and glc the supply of glucose. This metric suggests that R-cells were more efficient that S-cells ($y_S = 0.222 \pm 0.004$ normalised relative fluorescence units (nRFU) per mg of glucose in construct S, for $y_R = 0.305 \pm 0.013$ nRFU per mg of glucose in construct R; mean ± standard error with 8 replicates; Mann-Whitney U-test $p = 3.108 \times 10^{-4}$, ranksum = 37; Figure 1B). This observation is not surprising given that R also synthesises proteins coded in the plasmid with the same supply of glucose.

The second growth parameter to pGW155B carriage was the duration of the lag phase—time preceding active growth. However data here is less conclusive. According to fluorescence data, the lag phase was ~2h shorter in R-cells ($lag_S = 7.984 \pm 0.702$ hours *versus* $lag_R = 6.257 \pm 0.164$ hours, mean ± standard error with 8 replicates; Mann-Whitney U-test $p = 0.021$ with ranksum= 90; Figure 1B). However, optical density data suggested the opposite, with the lag for R-cells being nearly 4h longer than S's ($lag_S = 7.041 \pm 0.287$ hours

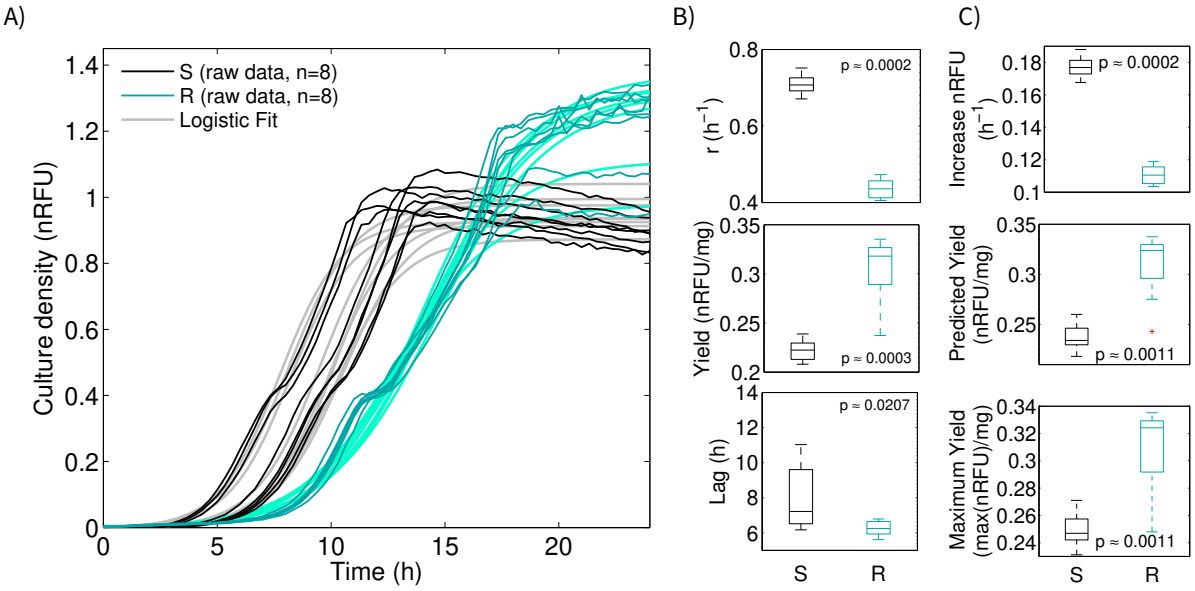

FIGURE 1. Asymmetric carriage costs of pGW155B. A) Overlapped growth curves of constructs S (black) and R (cyan) in the absence of tetracycline over 24h. I estimated the growth rate *per capita* (r), population size in the equilibrium (K), biomass yield, and lag duration from a 4-parameter logistic model fitted to growth data (see Methods). Data fits for constructs S and R are shown in grey and light cyan, respectively. **B)** Box plots showing the median (centre of the box), 25th and 75th percentile for each of the aforementioned parameters. The whiskers extend to the most extreme data points that are not outliers, and these are individually represented. The *p* value shown refers to a Mann-Whitney U-test (8 replicates) that I used to test differences in the parameters between both constructs. **C)** Alternative metrics for growth rate and biomass yield: Forward Euler approximation (top), data fit predicted yield (middle), and maximal yield across all time points in growth data (bottom). The *p* values correspond to Mann-Whitney U-tests (8 replicates).

versus $\text{lag}_R = 10.908 \pm 0.586$ hours; Mann-Whitney U-test $p = 1.554 \times 10^{-4}$ with ranksum=36; Figures S1B). Contrarily, in S-cells the lag was consistent between both datasets and did not change substantially. The metabolic alterations that plasmids introduce are still unclear (*28*–*32*), and pGW155B could possibly interfere with the production of CFP. To test this hypothesis, I tracked the relative change in fluorescence and optical density data. The ratio remained constant (Figure S5) as shown in prior data (*22*). Differences in the goodness of fit of the 4-parameter logistic model to fluorescence and optical density data (see Methods) is more likely explain the difference in lag of R-cells between fluorescence and optical density datasets. To circumvent similar issues with my estimates for biomass yield and growth rates, I measured them with alternative metrics. As Figures 1C and S1C illustrate, the variations in biomass yield and growth rate between both constructs are robust and consistent with those in Figure 1B.

Favouring high-yield enables co-maintenance of S- and R-cells, and plasmid persistence. To test whether fitness is a reliable metric for selection, I mixed equal proportions of two pure cultures of S and R, grown overnight, in media containing no antibiotic (see Methods). Then, I incubated this mixed culture at 30°C until *both* constructs reached their carrying capacity (K, ~ 24h as per data in Figure 1A). Finally, I propagated the mixed culture into a new plate containing fresh media and repeated the steps for seven days. As Figure 2A shows, this assays allowed the co-maintenance of both constructs despite their difference in fitness. I found the competitive exclusion of R, outcome predicted by population genetics theory, in only one replicate after seven days. Interestingly, the number of pGW155B in R-cells remained unchanged throughout the competition (Figure 2B, Mann-Whitney U-test $p = 0.1$ and ranksum= 15 for 3 replicates).

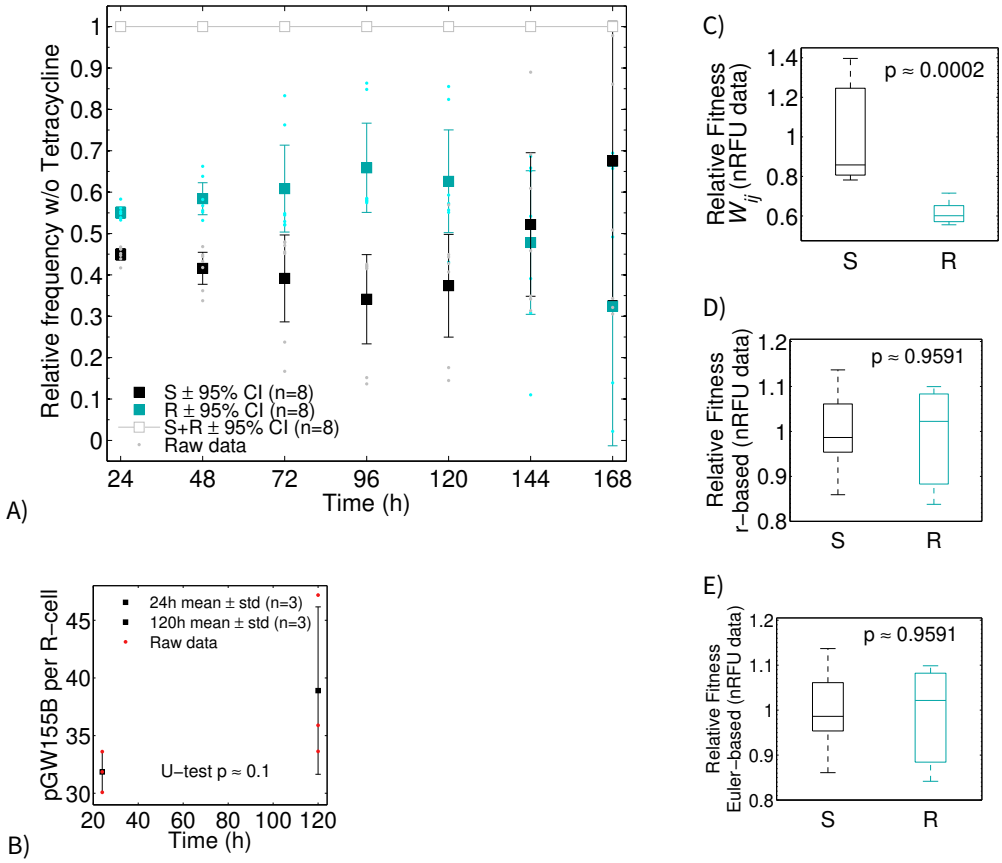

FIGURE 2. Co-maintenance of S and R without tetracycline not captured by classic fitness metric W_{ij}. A) Relative frequency of constructs S (black) and R (cyan) in mixed culture conditions without tetracycline. Error bars represent mean ± 95% confidence intervals, with 8 replicates. Raw data shown as dots. **B)** pGW155B copy number per R-cell from three representative replicates, measured using quantitative PCR (see Methods), after 24 and 120h of co-maintenance. Error bars represent mean ± standard deviation, and raw data is shown as red dots. The *p* value shown corresponds to a Mann-Whitney U-test used to measure significant differences in plasmid copy number. **C-E)** Box plot showing the median (centre of the box), 25th and 75th percentile for relative fitness using Malthusian growth rate (W_{ij}, C), growth rate *per capita* estimated from a 4-parameter logistic model (D), and forward Euler approximation (D, see main text). The whiskers extend to the most extreme data points that are not outliers. The *p* value shown corresponds to Mann-Whitney U-tests (8 replicates) to measure significant differences between the fitness in each construct.

How well does population genetics predict the outcome of this competition? Fitness competition assays, here between constructs S and R, are used to estimate fitness as (*4, 33*)

$$W_{ij} = m_i/m_j \tag{1}$$

where W_{ij} is the fitness of species i with respect to species j, and m is the growth rate of each species during the competition measured as Malthusian growth rate (m_i). It is noteworthy to mention that Malthusian growth assumes exponential, density-independent, growth rate. It is estimated by measuring the relative abundance of each species over time. For species i, for instance, the Malthusian growth rate is given by (*4*)

$$N_i(t) = N_i(0)e^{m_i t} \longrightarrow m_i = ln[N_i(t)/N_i(0)]/t \tag{2}$$

where $N_i(0)$ is the initial abundance of species i, $N_i(t)$ the abundance of species i at time t. Note that $N_i(0)$ must be positive and that $N_i(t) = N_i(0)$ when $t = 0$.

Thus, I applied equations 2 and 1 to calculate W_{RS} using data from the first 24h of competition and found that S-cells were approximately 35% fitter than R-cells (Mann-Whitney U-test $p = 1.554 \times 10^{-4}$ with ranksum= 100, 8 replicates; Figure 2C). The expectation would be, therefore, that S should obliterate R in prolonged competition akin to those in nature (*34*). But this is not what I found. As Figures 1A and S1A demonstrate, the core assumption of fitness, density-independent growth, is not met. Therefore, I recalculated W_{RS} using the growth rate estimates from a 4-parameter logistic model that I fitted to growth data of each construct in competition (see Methods), instead of using equation 2. The *new* fitness of S and R was now virtually the same (Figure 2D).

It can be reasonably argued that, for a subset of the data containing only the growth phase, density-independent growth can be a good approximation for growth rate. Indeed, growth rate is also calculated using linear regressions on logarithmic growth data, where Malthusian growth rate is given by the slope of the line fitted (*19, 20, 35, 36*). To eliminate the underlying conflict between the assumptions of density-dependent *versus* density-independent growth rates, I used a neutral metric: The forward Euler approximation (r_e). Applied to growth data of both constructs on competition, I defined r_e as

$$r_e = \max_{0 \le t \le 24h} \left[\frac{1}{D_i(t)} \cdot \frac{D_i(t + \Delta t) - D_i(t)}{\Delta t} \right] \tag{3}$$

where $D_i(t)$ is the growth data of species i—S or R—at time t, Δt the interval between reads in hours (0.3h), and $D_i(t + \Delta t)$ the growth data of species i at time $t + \Delta t$. Note that r_e has dimensions of t^{-1}. As defined, r_e shows how fast growth data changes over time and, in pure cultures, it was fastest in S-cells ($r_e = 0.177 \pm 0.002$ h^{-1} for construct S and $r_e = 0.111 \pm 0.002$ h^{-1} for construct R, mean ± standard error with 8 replicates; Mann-Whitney U-test $p = 1.554 \times 10^{-4}$ with ranksum = 100; Figure 1C). The result is, qualitatively, consistent with the growth rate estimate of the aforementioned 4-parameter logistic model. I also recalculated W_{RS} using the forward Euler approximation estimate, and the fitness of both S and R was virtually identical as Figure 2D shows.

Note that identical fitness for both R and S contradict data in Figure 1. This figure shows the growth dynamics of both constructs growing as pure cultures, however, fitness is estimated when both constructs *compete* in mixed cultures. Figure S6 shows that R-cells grow substantially faster in mixed culture (Mann-Whitney U-test $p = 3.108 \times 10^{-4}$, ranksum = 84; with 8 replicates), whereas the growth rate of S remained unchanged (Mann-Whitney U-test $p = 0.152$, ranksum = 43; with 8 replicates). The result is that both constructs have identical growth rate in mixed culture conditions (Mann-Whitney U-test $p \approx 1$, ranksum = 52; with 8 replicates), whence the same fitness. This variation in growth rate between pure culture and mixed culture conditions is consistent with prior data (*37–39*). The relative availability of glucose for each construct differs in mixed culture, as it is reasonable to expect, and growth rate is sensible to such variations (*18*).

III. Discussion

The co-maintenance between S- and R-cells should not be surprising. Contrary to population genetics, *rK selection theory* predicts that fitness and population size engage in a trade-off, and individuals with low relative fitness can thrive if selection favours population size (*16*). Prior data (*40*) and simulations (*41*) show this is, indeed, possible. However, evolutionary datasets are scarce. Perhaps more importantly, a key finding of my study is that R-cells preserved pGW155B—alongside its tetracycline-resistance gene. And this has practical implications.

First, resistant mutants (i.e. plasmid acquisition) incur costs, therefore, clinicians assume they will minimise, if not reverse, the emergence of resistance by reducing antibiotic exposure (*42–45*). This rationale is sound, but it has proven difficult in practice (*46, 47*). My data suggests reducing exposure alone may not be enough if fitness engages in trade-offs with other traits. Second, trade-offs between fitness and yield can jeopardise the detection of mutant selection windows and minimum inhibitory concentrations (see Supplementary Text I.A), as they will depend on the trait used to assess drug sensitivity: One trait may report costs of resistance, or plasmid carriage, whereas the other may not. And third, given the trade-off and additional yield of R-cells, selection of mutants with additional copies of pGW155B may occur well below the aforementioned mutant selection windows (see Supplementary Text I.B). Luckily, these trade-offs can be controlled (*18*) and therapies could exploit it.

IV. Methods

Media and Strains. I used the strains of *Escherichia coli* GB(c) and Wyl (*22*) (a gift from Remy Chait and Roy Kishony), and M9 minimal media supplemented with 0.4% glucose and 0.1% casamino acids (w/v). I made tetracycline stock solutions from powder stock (Duchefa, Ref. #0150.0025) at 5mg/mL in 50% ethanol, filter sterilised, and stored at -20^oC. Subsequent dilutions were made from this stock in supplemented M9 minimal media and kept at 4^oC.

Batch transfer protocol. I inoculated a 96-well microtitre plate containing 150µg/mL of supplemented M9 media with a mixture of two overnight cultures, one of *E. coli* GB(c) and another of *E. coli* Wyl (Figure S2). The overnight culture for GB(c) was supplemented with 100ng/mL of tetracycline to preserve the plasmid pGW155B carrying *tet(36)* (*35*), centrifuged and removed prior adding to the microtitre plate. I incubated the plate at 30^oC in a commercial spectrophotometer and measured the optical density of each well at 600nm (OD_{600}), yellow florescence for the S strain (YFP excitation at 505nm, emission at 540nm), and cyan fluorescence for the R strain (CFP at 430nm/480nm) every 20min for 24h. After each day I transferred 1.5µL of each well, using a 96-well pin replicator, into a new microtitre plate containing fresh growth medium and tetracycline.

Growth parameter estimation. Yellow and cyan fluorescence protein genes were constitutively expressed given the constant ratio between fluorescence and optical density (Figure S5). This enabled me to use fluorescence data as a proxy for cell density in mixed culture conditions. I normalised fluorescence readings using a conversion factor, n_f, calculated by growing each construct in a range of glucose concentrations, and regressing the linear model $RFU = n_f \cdot OD + c$ where RFU is relative fluorescence units data, OD optical density data, n_f the conversion factor between fluorescence and optical density, and c the crossing point with the y–axis when $OD = 0$.

I imported the resulting OD time series data set (Figures S3 and S4) into `MATLAB R2014b` to subtract background and calculate growth rate *per capita* (r) using the following algorithm. First, I fitted three mathematical models to data: 1) linear model $g(t) = b + r \cdot t$, 2) exponential model $g(t) = b + C \cdot \exp(r \cdot t)$ and 3) logistic model $g(t) = b + K/(1 + C \cdot \exp(-r \cdot [t - l]))$. The terms $g(t)$ denote culture growth through time (in OD, YFP, or CFP units), b the inoculum size used to subtract the background, C is a parameter, K the maximal population size attained and l the duration of the lag phase. I used the growth rate reported by the model with the lowest corrected Akaike Information Criterion (AICc). To estimate the biomass yield I

divided OD data in stationary phase by the glucose supplied (*27*). I also used the highest density across all time points and the density reported by the data fit, both divided by glucose supply, as alternative metrics for biomass yield.

Drug sensitivity parameter estimation. I defined the minimum inhibitory concentration (MIC or IC_{99}) for each trait as the tetracycline required to reduce the trait of the bacterium by a factor of 99%, compared to the tetracycline-free control. The MICs were 0.364 ± 0.012 (mean ± 95% confidence, 8 replicates), and 0.351 ± 0.013 of tetracycline for the strain S using culture density and growth rate, respectively. For the strain R they were 11.121 ± 1.735, and 9.113 ± 0.378 µg/mL.

DNA material extraction. For each concentration, I sampled three representative 150µg/mL replicates that I divided into two groups for chromosome and plasmid DNA extraction. I used 'GeneJet DNA' (ThermoScientific, Ref. #K0729) and 'GeneJet Plasmid' (ThermoScientific, Ref. #K0502) extraction kits to extract chromosomal and plasmid DNA (pDNA) from the samples, respectively, and used Qubit to quantify DNA and pDNA yields. Both extracts were diluted accordingly in extraction buffer, as per in manufacturer instructions, to normalise DNA across samples.

Quantitative PCR and plasmid copy number estimation. I used `primer3` to design two pairs of primers with melting temperature (T_m) of 60^oC and non-overlapping probes with T_m of 70^oC. The amplicon ranges between 100 to 141bp depending on the locus (Table 1). Two reaction mixes were prepared using the kit 'Luminaris Color Probe Low ROX' (ThermoScientific, Ref. #K0342), adding 0.3µM of each primer and 0.2µM of the probe as per manufacturer specifications. Following a calibration curve for each reaction (Figure S9) I added 0.01ng of chromosomal or plasmid DNA material to each of the reaction mixes.

TABLE 1. Primers and probes designed using `Primer3`. Amplicon ranging from 100 to 141bp. T_m indicates the estimated melting temperature.

Target gen	Sequence ($5' \rightarrow 3'$)	T_m (^oC)	Feature
tatB	CGATGAAGCGTTCCTACGTT	60.27	Forward
	TCATGCGCAGCTTCATTATC	59.94	Reverse
	AAGGCGAGCGATGAAGCGCA	70.70	Probe
tet(36)	ATTGGGCATCTATTGGCTTG	59.22	Forward
	CCGATTCACAGGCTTTCTTG	60.76	Reverse
	AGCCTTTGCCAATTGGGGCG	70.37	Probe

To estimate the relative copies of pGW155B per R cell, I calculated the corresponding proportion of chromosomal DNA corresponding to the R-type from data in Figure S10D and used the formula (*48*)

$$cn = \frac{(1+E_c)^{Ctc}}{(1+E_p)^{Ctp}} \times \frac{S_c}{S_p},$$

where cn is the number of plasmid copies per chromosome, S_c and S_p are the size of the chromosome and pGW155B amplicon in bp, E_c and E_p the efficiency of the qPCR taken from data in Figure S9, and Ctc and Ctp are the cycles at which I first detected product amplification (C_t).

Competing interests

The author declares no competing interests.

References

1. Orr, H. A. Fitness and its role in evolutionary genetics. *Nat. Rev. Genet.* **10,** 531–539 (2009).
2. Hamilton, M. *Population Genetics* ISBN: 9781444362459 (Wiley, 2011).
3. Fisher, R. A. *The Genetical Theory of Natural Selection* 308–315 (At The Clarendon Press, 1930).
4. Lenski, R. E., Rose, M. R., Simpson, S. C. & Tadler, S. C. Long-Term Experimental Evolution in Escherichia coli. I. Adaptation and Divergence During 2,000 Generations. *Am. Nat.* **138,** pp. 1315–1341 (1991).
5. Pontarotti, P. *Evolutionary Biology: Exobiology and Evolutionary Mechanisms.* ISBN: 9783642382123 (Springer Berlin Heidelberg, 2013).
6. Andersson, D. I. & Levin, B. R. The biological cost of antibiotic resistance. *Curr. Opin. Microbiol.* **2,** 489–493 (1999).
7. Lipsitch, M., Bergstrom, C. T. & Levin, B. R. The epidemiology of antibiotic resistance in hospitals: Paradoxes and prescriptions. *Proc. Natl. Acad. Sci. U.S.A.* **97,** 1938–1943 (2000).
8. Bergstrom, C. T., Lo, M. & Lipsitch, M. Ecological theory suggests that antimicrobial cycling will not reduce antimicrobial resistance in hospitals. *Proc. Natl. Acad. Sci. U.S.A.* **101,** 13285–90 (2004).
9. Wang, Y. C. & Lipsitch, M. Upgrading antibiotic use within a class: tradeoff between resistance and treatment success. *Proc. Natl. Acad. Sci. U.S.A.* **103,** 9655–9660 (2006).
10. McAdams, D., Wollein Waldetoft, K., Tedijanto, C., Lipsitch, M. & Brown, S. P. Resistance diagnostics as a public health tool to combat antibiotic resistance: A model-based evaluation. *PLoS Biol.* **17,** e3000250 (2019).
11. Ram, Y., Dellus-Gur, E., Bibi, M., *et al.* Predicting microbial growth in a mixed culture from growth curve data. *Proc. Natl. Acad. Sci. U.S.A.* **116,** 14698–14707 (2019).
12. Quer, J., Huerta, R., Novella, I. S., *et al.* Reproducible nonlinear population dynamics and critical points during replicative competitions of RNA virus quasispecies. *J. Mol. Biol.* **264,** 465–471 (1996).
13. Haymer, D. S. & Hartl, D. L. The experimental assessment of fitness in Drosophila. I. Comparative measures of competitive reproductive success. *Genetics* **105,** 455–466 (2008).
14. Fleming, T. H., Maurice, S., Buchmann, S. L. & Tuttle, M. D. Reproductive Biology and Relative Male and Female Fitness in a Trioecious Cactus, Pachycereus pringlei (Cactaceae). *Am. J. Bot.* **81,** 858–867 (1994).
15. Orr, H. A. The population genetics of beneficial mutations. *Philos. Trans. R. Soc. Lond., B, Biol. Sci.* **365,** 1195–1201 (2010).
16. MacArthur, R. H. Some generalized theorems of natural selection. *Proc. Natl. Acad. Sci. U.S.A.* **48,** 1893 (1962).
17. Reznick, D., Bryant, M. J. & Bashey, F. r-and K-selection revisited: the role of population regulation in life-history evolution. *Ecology* **83,** 1509–1520 (2002).
18. Reding-Roman, C., Hewlett, M., Duxbury, S., *et al.* The unconstrained evolution of fast and efficient antibiotic-resistant bacterial genomes. *Nat. Ecol. Evol.* **1,** 0050 (2017).

19. Ow, D. S.-W., Nissom, P. M., Philp, R., Oh, S. K.-W. & Yap, M. G.-S. Global transcriptional analysis of metabolic burden due to plasmid maintenance in Escherichia coli DH5α during batch fermentation. *Enzyme. Microb. Technol.* **39,** 391–398 (2006).

20. Van Rensburg, E., Den Haan, R., Smith, J., van Zyl, W. H. & Görgens, J. F. The metabolic burden of cellulase expression by recombinant Saccharomyces cerevisiae Y294 in aerobic batch culture. *Appl. Microbiol. Biotechnol.* **96,** 197–209 (2012).

21. Vogwill, T. & MacLean, R. C. The genetic basis of the fitness costs of antimicrobial resistance: a meta-analysis approach. *Evol. Appl.* **8,** 284–295 (2015).

22. Chait, R., Shrestha, S., Shah, A. K., Michel, J.-B. & Kishony, R. A Differential Drug Screen for Compounds That Select Against Antibiotic Resistance. *PLoS One* **5,** e15179 (2010).

23. Whittle, G, Whitehead, T. R., Hamburger, N, Shoemaker, N. B., Cotta, M. A., *et al.* Identification of a new ribosomal protection type of tetracycline resistance gene, tet(36), from swine manure pits. *Appl. Environ. Microbiol.* **64,** 4151–4158 (2003).

24. Smillie, C., Garcillán-Barcia, M. P., Francia, M. V., Rocha, E. P. & de la Cruz, F. Mobility of plasmids. *Microbiol. Mol. Biol. Rev.* **74,** 434–452 (2010).

25. Garcillán-Barcia, M. P., Alvarado, A. & de la Cruz, F. Identification of bacterial plasmids based on mobility and plasmid population biology. *FEMS Microbiol. Rev.* **35,** 936–956 (2011).

26. Stevenson, K., McVey, A. F., Clark, I. B., Swain, P. S. & Pilizota, T. General calibration of microbial growth in microplate readers. *Sci. Rep.* **6,** 1–7 (2016).

27. Monod, J. The Growth of Bacterial Cultures. *Annu. Rev. Microbiol.* **3,** 371–394 (1949).

28. Rhee, J. I., Ricci, J. C. D., Bode, J. & Schügerl, K. Metabolic enhancement due to plasmid maintenance. *Biotechnol. Lett.* **16,** 881–884 (1994).

29. Diaz Ricci, J. C. & Hernández, M. E. Plasmid effects on Escherichia coli metabolism. *Crit. Rev. Biotechnol.* **20,** 79–108 (2000).

30. Gonçalves, G. A., Bower, D. M., Prazeres, D. M., Monteiro, G. A. & Prather, K. L. Rational engineering of Escherichia coli strains for plasmid biopharmaceutical manufacturing. *Biotechnol. J.* **7,** 251–261 (2012).

31. Baltrus, D. A. Exploring the costs of horizontal gene transfer. *Trends Ecol. Evol.* **28,** 489–495 (2013).

32. San Millan, A. Evolution of Plasmid-Mediated Antibiotic Resistance in the Clinical Context. *Trends Microbiol.* (2018).

33. Travisano, M. & Lenski, R. E. Long-term experimental evolution in Escherichia coli. IV. Targets of selection and the specificity of adaptation. *Genetics* **143,** 15–26 (1996).

34. Hibbing, M. E., Fuqua, C., Parsek, M. R. & Peterson, S. B. Bacterial competition: surviving and thriving in the microbial jungle. *Nat. Revs. Microbiol.* **8,** 15–25 (2010).

35. Chait, R., Craney, A & Kishony, R. Antibiotic interactions that select against resistance. *Nature* **446,** 668–671 (2007).

36. Starikova, I., Sørum, V., Johnsen, P. J., *et al.* Fitness costs of various mobile genetic elements in Enterococcus faecium and Enterococcus faecalis. *J. Antimicrob. Chemother.* **68,** 2755–2765 (2013).

37. Chaia, A. P., Strasser de Saad, A., de Ruiz Holgado, A. P. & Oliver, G. Competitive inhibition of propionibacterium acidipropionici by mixed culturing with Lactobacillus helveticus. *J. Food Prot.* **57,** 341–344 (1994).

38. Hirayama, K. *et al.* Effects of bacterial coexistence on the growth of a marine diatom Chaetoceros gracilis. *Fish. Sci.* **62,** 40–43 (1996).

39. Rüger, M., Ackermann, M. & Reichl, U. Species-specific viability analysis of Pseudomonas aeruginosa, Burkholderia cepacia and Staphylococcus aureus in mixed culture by flow cytometry. *BMC Microbiol.* **14,** 56 (2014).

40. Mueller, L. D. & Ayala, F. J. Trade-off between r-selection and K-selection in Drosophila populations. *Proc. Natl. Acad. Sci. U.S.A.* **78,** 1303–1305 (1981).

41. Kurihara, Y., Shikano, S. & Toda, M. Trade-off between interspecific competitive ability and growth rate in bacteria. *Ecology* **71,** 645–650 (1990).

42. Livermore, D. M. Minimising antibiotic resistance. *Lancet Infect. Dis* **5,** 450–459 (2005).

43. Zur Wiesch, P. A., Kouyos, R., Engelstädter, J., Regoes, R. R. & Bonhoeffer, S. Population biological principles of drug-resistance evolution in infectious diseases. *Lancet Infect Dis* **11,** 236–47 (Mar. 2011).

44. Holmes, A. H., Moore, L. S., Sundsfjord, A., *et al.* Understanding the mechanisms and drivers of antimicrobial resistance. *The Lancet* **387,** 176–187 (2016).

45. Buckner, M. M., Ciusa, M. L. & Piddock, L. J. Strategies to combat antimicrobial resistance: anti-plasmid and plasmid curing. *FEMS Microbiol. Rev.* **42,** 781–804 (2018).

46. Sundqvist, M., Geli, P., Andersson, D. I., *et al.* Little evidence for reversibility of trimethoprim resistance after a drastic reduction in trimethoprim use. *J. Antimicrob. Chemother.* **65,** 350–360 (Nov. 2009).

47. Sundqvist, M. Reversibility of antibiotic resistance. *Ups J Med Sci* **119,** 142–148 (2014).

48. Millán, A. S., Peña-Miller, R., Toll-Riera, M, *et al.* Positive selection and compensatory adaptation interact to stabilize non-transmissible plasmids. *Nat. Commun.* **5** (2014).

I. Supplementary Text

I.A. 'Mutant Selection Window' (MSW) hypothesis sensitive to asymmetries in carriage costs.

Deciding whether pGW155B is costly can be problematic, given my results. This uncertainty has practical implications, particularly for clinicians and evolutionary biologists. The notion of 'selection window' is fundamental for clinical therapies designed to minimise the emergence of resistant mutants. The 'mutant selection window' (MSW) hypothesis states (*1*–*3*) that resistant mutants emerge within a specific range of drug concentrations: between the minimal selective concentration (MSC) (*3*), sub-inhibitory, and the mutant prevention concentration (MPC) (*4*), supra-inhibitory. By definition (*1*), no resistant mutant emerges above or below these concentrations. But there is an inconsistency in how MSC and MPC are estimated.

The MPC is based on whether microbes form colonies on Petri dishes containing a range of drug concentrations. Its interpretation is binary, either the colonies form or they do not (*2*). The MSC, on the other hand, relies on growth rate data (*3, 5, 6*). And here is where the asymmetry of carriage costs is relevant. The MSC assumes that resistant microbes, either by chromosomal mutations or plasmid carriage, divide at slower rates than their sensitive counterparts (*3, 6, 7*). Thus, when resistant and sensitive microbes are exposed to the same range of drug concentrations, there is a concentration at which both microbes have identical growth rate, given their different sensitivities: The MSC. The resistant type will therefore divide faster at concentrations above the MSC, whereas below it the sensitive type divides faster. In other words, drug-sensitive microbes outgrow resistant mutants below the MSC and *vice versa*. Given the similarity of this rationale to that for plasmid persistence, I asked whether MSCs can reliably predict the selection of mutants harbouring plasmids with antibiotic resistance genes. As Figure 2A suggests, it does not.

To estimate the MSC I first needed to expose the constructs S and R to tetracycline, calculate the growth rate for each construct grown in each concentration (see Methods), and determine their dose-response profiles (Figure S10A). Note that MSCs are calculated by overlapping the dose-response of each construct grown separately as pure cultures (*3*). Consistently with the assumption behind the MSC, the construct R grew 0.27 ± 0.015 h^1 slower than S in the absence of tetracycline (mean ± standard error with 8 replicates; Mann-Whitney U-test $p = 1.554 \times 10^{-4}$, ranksum = 100). This means there must be a concentration at which both constructs have identical growth rates and the dose-response profiles cross: 0.066 ± 0.004 µg/mL of tetracycline.

To answer whether MSCs predict the selection of drug-resistant mutants harbouring plasmids, I mixed equal proportions of two pure cultures of each construct—grown overnight—and exposed them to increasing tetracycline concentrations. These concentrations are constrained by S, the most sensitive strain, as using concentrations above its IC_{99} (concentration inhibiting 99% its growth rate) are equivalent to pure cultures of R as Figure S10A illustrates. As above, I propagated the mixed culture into a new plate containing fresh media and antibiotic after 24h of growth, and repeated the transfers for seven days. I tracked daily changes in MSC, but they were not significant (Kruskal-Wallis H-test $p = 0.446$ and χ^2−statistic = 5.795 with 8 replicates, Figure S10B). It is therefore reasonable to expect that construct R would grow faster above the MSC, and construct S below the MSC—consistently with (*3*). However, given the yield benefits of pGW155B, R-cells outnumbered S even below the minimal selective concentration (Figure S7).

I calculated the selection coefficient (*8*), s, for the construct R as

$$s = \frac{ln\left[r_i(t)/r_i(0)\right]}{t} \tag{4}$$

where $r_i(0)$ is the initial ratio of species i—here the construct R—and $r_i(t)$ the ratio of i at time t. Selection for species i is denoted by coefficients above zero ($0 < s$), whereas coefficients below zero ($0 > s$) imply selection against i. Consistently with my previous finding, $s \approx 0$ for R when the mixed culture was not exposed to tetracycline (Figure S10C). But it was significantly positive at any drug concentration used: For 0.02 µg/mL of tetracycline, the lowest concentration I used, $s = 0.0095 \pm 0.003\ \mathrm{h}^{-1}$ (Mann-Whitney U-test against 0 µg/mL $p = 0.007$, ranksum= 32 with 8 replicates). This concentration is well below its IC_{99} (9.113 ± 0.378 µg/mL of tetracycline, mean ± 95% confidence with 8 replicates, Figure S10A) and, most importantly, the minimal selective concentration (MSC). It can be argued that equation 4 above relies on cell number only. A similar metric exists (*9, 10*) for Malthusian growth rates, where the selection coefficient of species i with respect to species j is given by

$$s'_{ij} = \frac{m_i - m_j}{m_j} = W_{ij} - 1 \tag{5}$$

where m_i and m_j is the Malthusian growth rate of species i and j, respectively, and W_{ij} the fitness of species i with respect to j (see equation 1). Note that this expression is independent of time. Figure S10D illustrates s'_{RS} in all tetracycline concentrations used. The prediction is, indeed, compatible with the rationale behind the minimal selective concentration. But it fails to explain the persistence of construct R below the MSC, despite its negative selection coefficient.

The difference in errorbar size in Figures S10C, S10D and S7 suggests the likely emergence of mutants in either construct. Given the identical genetic background of both constructs (*Escherichia coli* MC4100, where pGW155B and fluorescence markers are the only differences), I used quantitative PCR to measure the relative abundance of pGW155B in R-cells (see Methods) and found that R-cells exposed to more tetracycline bore more copies of the plasmid. As I describe in Supplementary Text I.B, pGW155B lacks partition mechanisms and its persistence relies on stochastic segregation during cell division. I developed a mathematical model (see Supplementary Text I.B) supporting that the increase in pGW155B that I observed is compatible with imperfect segregation events.

I.B. Tetracycline-resistant mutants with additional copies of pGW155B can be selected below the minimal selective concentration (MSC).

The drug concentrations that I used suppose 0.2% to 2% the minimum inhibitory concentration for the construct R (see Figure S10A in main text). Despite the relatively low tetracycline used, Figure S11A reveals substantial changes in the growth rate of R between the first and last day of the experiment (linear regression $p \approx 1.45 \times 10^{-4}$, F-statistic= 16.7, adjusted coefficient of determination $R^2 = 0.222$; slope parameter 1.876, $p \approx 1.99 \times 10^{-4}$, t-statistic= 3.9915; 8 replicates). It is reasonable to expect an increase in growth rate as R adapts to the growth conditions—the same for seven consecutive days. However, I found a concomitant change in yield and lag—redolent of the asymmetric costs of pGW155B shown in the main text, in Figure 1 (Figures S11B and C). Given the experimental setup, it is difficult to expose chromosomal mutations in both, R and S, and underpin those that ease pGW155B carriage (see main text). Thus, I asked whether the number of plasmids borne by R cells changed over time with different tetracycline concentrations—it did.

To quantify the relative abundance of pGW155B within R cells, I sampled representative cultures on days one and five, calculated the proportion of chromosomal DNA corresponding to the construct R, and used quantitative polymerase chain reaction (qPRC) to measure the number of plasmids borne per cell (see Methods). The initial pool of cells from this strain, grown overnight in pure culture and used to in-

oculate the mixed cultures, contained 30.21 ± 6.72 copies of pGW155B per cell (mean ± 95% confidence, $n = 3$). Without tetracycline, the number of pGW155B did not change significantly after one and five days of competition against S (Mann-Whitney U-test $p = 0.1$ and ranksum = 15 with 3 replicates, Figure S11D). However, the relative abundance of pGW155B changed rapidly with increasing drug concentrations: I observed a 2-fold increase in the number of plasmids hosted by R within 24h, and 6- to 10-fold after five days of depending on tetracycline concentration (Figures S11E and F).

To understand the variation in plasmid copy number with respect to drug concentration, I fitted two mathematical models to qPCR data. First, the linear model $p_c = p_0 + d\kappa$ and the constant model $p_c = \kappa$, where κ denotes the slope or proportionality constant, p_0 the initial number of copies borne by each R cell and d the antibiotic supplied. The constant model assumes no change in the number of plasmids borne, and it was extremely unlikely (relative likelihood with respect to the linear model ≈ 0.034, Figure S11E). Instead, the linear model suggests that plasmid copy number correlates with drug concentration, where the constant of proportionality $\kappa = 161.87 \pm 110.37$ plasmids per mL per microgram of drug per cell (t-statistic = 2.874, $p = 0.009$ and 95% confidence interval (45.08, 278.662)). Albeit significant, with an adjusted coefficient of determination (R^2) of 0.246, the linear model does not entirely capture the changes observed in qPCR data. A switch-like, non-linear model, say, the logistic model (see Methods), explained better the variation in the number of pGW155B that I observed (adjusted R^2 of 0.472). After five days of exposure to tetracycline, the constant κ increased from 161.87 ± 110.37 to 880.19 ± 705.71 plasmids per mL per microgram of drug per cell (Figure S11F, t-statistic = 2.4446, $p = 0.0229$, and 95% confidence interval (133.5, 1626.9)). The predictive power declined for the logistic model, albeit it was still better than that for the linear model (adjusted $R^2 = 0.411$ *versus* 0.261).

Tetracycline skews random segregation of pGW155B during cell division. Now the question is this: how did R cells gain additional copies of pGW155B? The plasmid lacks a *rep* gene to control tightly the partition of plasmids after cell division (*11*–*13*) (addgene vector database accession #2853). While pGW155B is a synthetic plasmid, many natural plasmids also lack partition systems (*13*, *14*) so I hypothesised the following: That random segregation, the mechanism underlying plasmids loss in the absence of selection (*15*), can also facilitate their accumulation in bacteria. Exposure to tetracycline would, therefore, skew the segregation of plasmids to favour daughter cells with additional copies of pGW155B.

Suppose a microbe that harbours a non-transmissible plasmid, and neither the microbe's chromosome nor the plasmid can mutate. The plasmid imposes a cost $0 < \Gamma < 1$ on the microbe's growth rate, and the cost is proportional to the number of plasmids hosted as we may expect. Now, if the microbe bears n copies of the plasmid and it replicates alongside the host's chromosome, the only means to gain or lose plasmids would be through the imperfect segregation of plasmids during cell division: One daughter cell would carry $n + 1$ plasmids whereas the other is left with $n - 1$. This process is how pGW155B, I hypothesise, changed its relative abundance in *E. coli*.

Let me assume these imperfect segregations are a Markov process, where they occur with a probability σ and are independent of previous imperfect segregation events. For simplicity, I assume that only one plasmid can be gained or lost during each imperfect segregation. Note that, regardless of the initial number of plasmids present in the inoculum, j subpopulations will emerge—containing from 0 to $j - 1$ copies—derived from this rationale as I show below. Thus, the population of the aforementioned microbe is given by the time-series vector $\mathbf{B}(t, A, S) = (b_1(t, S, A), b_2(t, S, A), \ldots, b_j(t, S, A))$. This vector contains the density of j different subpopulations of the same genotype, but hosting different number of plasmids, that sum

together to form B at time t given a carbon source S and an antibiotic A. To make the model compatible with the batch transfer protocol used in this study, I further assume that $\mathbf{B}$ is transferred to an environment with replenished S and A at fixed time intervals, k, usually at 24h, satisfying the expression

$$\mathbf{B}_k(t_0, S_0, A_0) = \eta \cdot \mathbf{B}_{k-1}(t_{k-1}, S_{k-1}, A_{k-1})$$

where $0 < \eta \ll 1$ denotes the fraction transferred (typically $\eta = 0.01$). Given the above assumptions, the resulting probability matrix for the Markov process (M) is

$$M = \begin{pmatrix} 1 & \sigma & 0 & & \cdots & 0 \\ 0 & 1-2\sigma & \sigma & 0 & & \vdots \\ 0 & \sigma & 1-2\sigma & \sigma & \ddots & \\ & 0 & \sigma & 1-2\sigma & \ddots & 0 \\ \vdots & & \ddots & \ddots & \ddots & \sigma \\ 0 & \cdots & & 0 & 0 & 1-\sigma \end{pmatrix}.$$

Although only one plasmid can be gained or lost in each imperfect segregation event, cells that lose all their plasmids cannot recover them (i.e. cells that only host one plasmid) and these cells become sensitive to the antibiotic A. Now, the column vector $\mathbf{U}(S) = (U(b_1, S), U(b_2, S), \ldots, U(b_j, S))$ of uptake rates of all subpopulations is determined by the Monod function

$$U(b, S) = V^{max} \frac{bS}{k_m(b) + S}.$$

The maximum uptake rate is given by V^{max}, and $k_m(b_n)$ is the associated half-saturation constant for cells of the n-th subpopulation where $k_m(b_n)$ is a smooth function. Let me now define c_n as the biomass yield of cells from the n-th subpopulation, where c_n can be derived from the maximal uptake rate of cells in subpopulation n. This can be written as $c_n = c(b_n)$, where $c(\cdot)$ is a smooth function. The growth rate of each subpopulation is given by the vector $\mathbf{G}(S, A) = (G(b_1, S, A), G(b_2, S, A), \ldots, G(b_j, S, A))$ at carbon concentration S, where

$$G(b, S, A) = c(b) \cdot U(b, S) \cdot (1 - \Gamma) \cdot \frac{1}{1 + \kappa(b)A^2}.$$

Note that $\mathbf{G}(S, A)$ is modulated by the costs imposed by plasmid carriage Γ, and the antibiotic A. The term $\frac{1}{1+\kappa(b)A^2}$ describes the inhibition exerted by the drug on the n-th subpopulation of B (b_n), where $\kappa(b_n)$ is the affinity of the antibiotic for its substrate and 2 is the Hill coefficient. The following system of ordinary differential equations describe the change in $\mathbf{B}$ over time, given S and A

$$\frac{d\mathbf{B}}{dt} = M\Big((1 - \Gamma) \cdot \mathbf{G}(S, A_0) \circ \mathbf{B}\Big), \tag{6a}$$

$$\frac{dA_i}{dt} = -d \cdot A_i + \phi \cdot (A_e - A_i) \cdot \sum_{n=1}^{j} b_n, \tag{6b}$$

$$\frac{dA_e}{dt} = -d \cdot A_e - \phi \cdot (A_e - A_i) \cdot \sum_{n=1}^{j} b_n, \tag{6c}$$

$$\frac{dS}{dt} = -\langle \mathbf{U}(S), \mathbf{B} \rangle, \tag{6d}$$

where $\langle \mathbf{U}(S), \mathbf{B} \rangle$ represents the Euclidean inner product of two vectors of the same dimension, $\langle \boldsymbol{u}, \boldsymbol{v} \rangle = \sum_{n=1}^{j} u_n v_n$. Finally, the carbon uptake follows Michaelis-Menten kinetics (see above), but the antibiotic A diffuses from the environment (A_e) into the cells (A_i) with a rate ϕ.

Figures S12A and B illustrate the qualitative change in population structure resulting from the exposure of B to the antibiotic A. When the microbe grows in the absence of drug, the subpopulation with fewer copies of the plasmid is favoured given their lower relative costs. In this condition, cells harbouring more copies are rare. However, the distribution changes when the microbe is exposed to A: More copies of the plasmid are needed to overcome the antibiotic challenge. Crucially, with more antibiotics, subpopulations hosting higher number of copies are favoured—despite the costs of plasmid carriage.

The experimental data set is consistent with this prediction (Figures S12C, D and E). If the initial pool of *E. coli* cells contained 30.21 ± 6.72 copies of the plasmid, after 24h of antibiotic challenge cells containing more copies rapidly emerged. To find the distribution that best fits the data, I tried all distributions available in `MATLAB 2014a` using the built-in routine `fitdist`. Then, I used the negative log-likelihood (NLogL) function and corrected Akaike Information Criterion (AICc) as metrics for the goodness of fit, and sorted the distributions accordingly. I considered the best distribution to be that with the lowest NLogL and AICc. After 24h of exposure to tetracycline, the data followed a Nakagami distribution (corrected Akaike Information Criterion AICc = 198.14, Negative Log-Likelihood $NLogL = 96.79$) with parameters for shape $\mu = 2.18$ and scale $\omega = 1.79 \times 10^3$ (95% confidence intervals are $\mu = (1.29, 3.71)$ and $\omega = (1367.1, 2348.9)$). The mean copies of plasmids borne per cell after this period were 39.95 ± 10.58 (mean ± 95% confidence).

These parameters changed when I prolonged the antibiotic challenge. After 120h of exposure to tetracycline the mean copies per cell increased to 169.58 ± 90.14 and the data now followed a skewed BirnbaumSaunders distribution (AICc = 290.19, NLogL = 142.81 *versus* AICc = 293.66 and NLogL = 144.54 for the Nakagami distribution) with parameters for shape $\gamma = 0.73$ and scale $\beta = 133.52$ (95% confidence $\gamma = (97.07, 169.98)$ and $\beta = (0.52, 0.94)$). Thus, the antibiotic challenge increased the frequency of cells bearing more copies of pGW155B consistently with this theory (Figure S12E) where the imperfect segregation of plasmid during cell division would be the underlying mechanism.

Supplementary References

1. Baquero, F. & Negri, M.-C. Challenges: Selective compartments for resistant microorganisms in antibiotic gradients. *Bioessays* **19,** 731–736 (1997).
2. Zhao, X. & Drlica, K. Restricting the selection of antibiotic-resistant mutants: a general strategy derived from fluoroquinolone studies. *Clin. Infect. Dis.* **33,** S147–S156 (2001).
3. Gullberg, E., Cao, S., Berg, O. G., *et al.* Selection of resistant bacteria at very low antibiotic concentrations. *PLoS Pathog.* **7,** e1002158 (July 2011).
4. Drlica, K. & Zhao, X. Mutant selection window hypothesis updated. *Clin. Infect. Dis.* **44,** 681–8 (Mar. 2007).
5. Rosenbloom, D. I., Hill, A. L., Rabi, S. A., Siliciano, R. F. & Nowak, M. A. Antiretroviral dynamics determines HIV evolution and predicts therapy outcome. *Nat. Med.* **18,** 1378–1385 (2012).
6. Day, T., Huijben, S. & Read, A. F. Is selection relevant in the evolutionary emergence of drug resistance? *Trends Microbiol.* **23,** 126–133 (2015).
7. Andersson, D. I. & Levin, B. R. The biological cost of antibiotic resistance. *Curr. Opin. Microbiol.* **2,** 489–493 (1999).
8. Travisano, M. & Lenski, R. E. Long-term experimental evolution in Escherichia coli. IV. Targets of selection and the specificity of adaptation. *Genetics* **143,** 15–26 (1996).
9. Kimura, M. On the change of population fitness by natural selection. *Heredity* **12,** 145–167 (1958).
10. Lenski, R. E., Rose, M. R., Simpson, S. C. & Tadler, S. C. Long-Term Experimental Evolution in Escherichia coli. I. Adaptation and Divergence During 2,000 Generations. *Am. Nat.* **138,** pp. 1315–1341 (1991).
11. Del Solar, G. & Espinosa, M. Plasmid copy number control: an ever-growing story. *Mol. Microbiol* **37,** 492–500 (2000).
12. Garcillán-Barcia, M. P., Alvarado, A. & de la Cruz, F. Identification of bacterial plasmids based on mobility and plasmid population biology. *FEMS Microbiol. Rev.* **35,** 936–956 (2011).
13. Million-Weaver, S. & Camps, M. Mechanisms of plasmid segregation: have multicopy plasmids been overlooked? *Plasmid* **75,** 27–36 (2014).
14. Guynet, C. & de la Cruz, F. Plasmid segregation without partition. *Mob. Genet. Elements* **1,** 236–241 (2011).
15. Millán, A. S., Peña-Miller, R., Toll-Riera, M, *et al.* Positive selection and compensatory adaptation interact to stabilize non-transmissible plasmids. *Nat. Commun.* **5** (2014).

II. Supplementary Figures

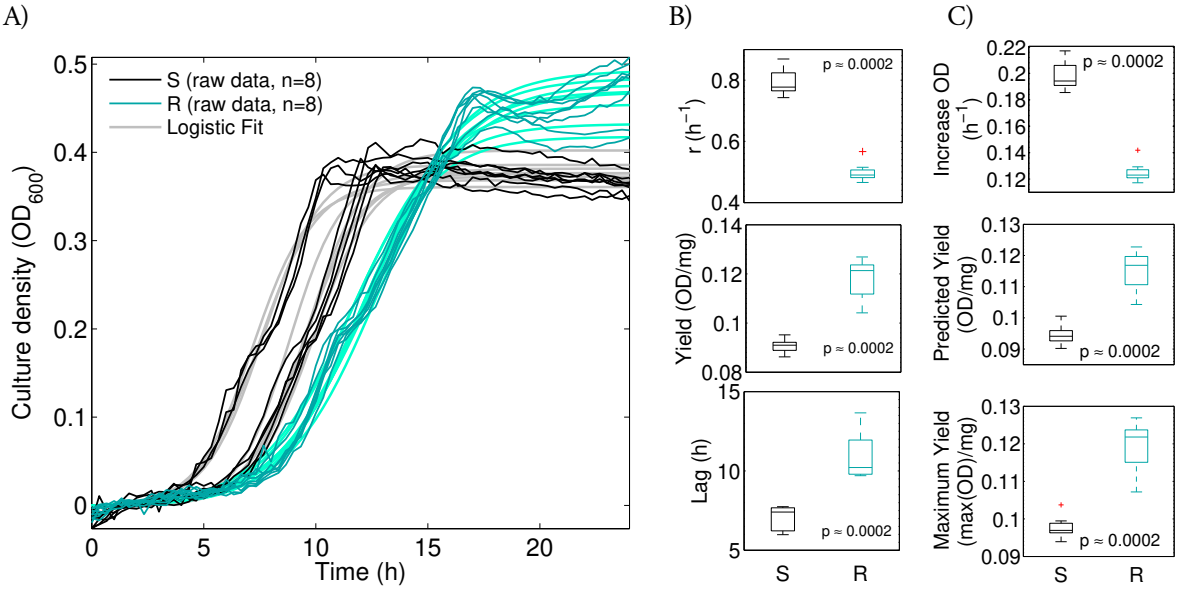

Figure S1. Asymmetric carriage costs of pGW155B (optical density data). A) Overlapped growth curves of constructs S (black) and R (cyan) in the absence of tetracycline over 24h. I estimated the growth rate *per capita* (r), population size in the equilibrium (K), biomass yield, and lag duration from a 4-parameter logistic model fitted to growth data (see Methods). Data fits for constructs S and R are shown in grey and light cyan, respectively. **B)** Box plots showing the median (centre of the box), 25th and 75th percentile for each of the aforementioned parameters. The whiskers extend to the most extreme data points that are not outliers, and these are individually represented. The *p* value shown refers to a Mann-Whitney U-test (8 replicates) that I used to test differences in the parameters between both constructs. **C)** Alternative metrics for growth rate and biomass yield: Forward Euler approximation (top), data fit predicted yield (middle), and maximal yield across all time points (bottom). The *p* values correspond to Mann-Whitney U-tests (8 replicates).

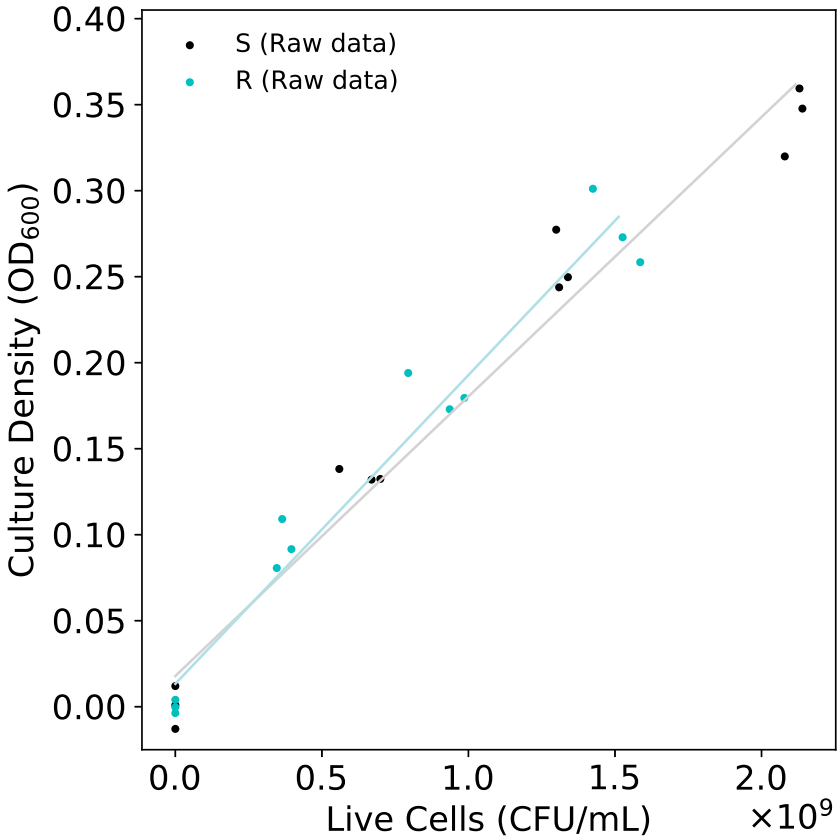

Figure S2. Calibration curve to translate optical density data to number of *Escherichia coli* cells. I fitted the linear model $a = bx + c$ to optical density and colony counting data (dots) to calculate the number of optical density units (OD_{600}) per cell. a denotes the optical density readings measured at 600nm, c the crossing point with the y−axis when $x = 0$, and b the conversion factor between optical density and number of cells (x). I interpolating optical density readings to calculate the number of cells within a culture as $x = (a - c)/b$. For the strain S, $b = 1.62 \times 10^{-10}\ OD \cdot mL \cdot CFU^{-1}$ and $c = 1.78 \times 10^{-2}\ OD$, whereas for R $b = 1.79 \times 10^{-10}\ OD \cdot mL \cdot CFU^{-1}$ and $c = 1.33 \times 10^{-2}\ OD$.

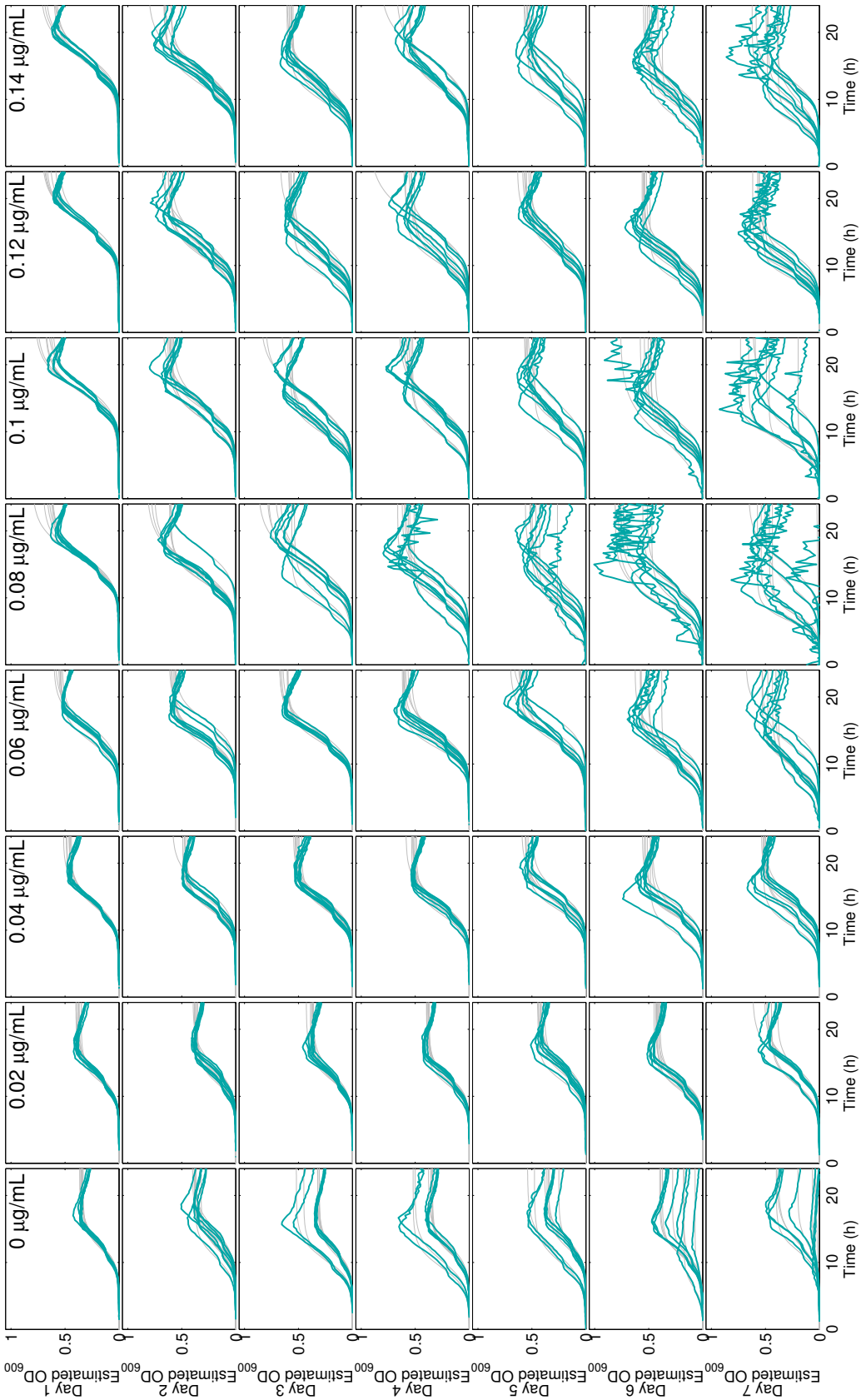

Figure S3. Raw data and model fit for resistant R strain in mixed culture conditions. Raw optical Density data for GB(c) measured every 20min for seven days (blue). The best fit to data (see Methods in main text) used to calculate bacterial fitness is shown in grey. Each column represents one day worth of data for a given condition, and each row the data set for one tetracycline concentration.

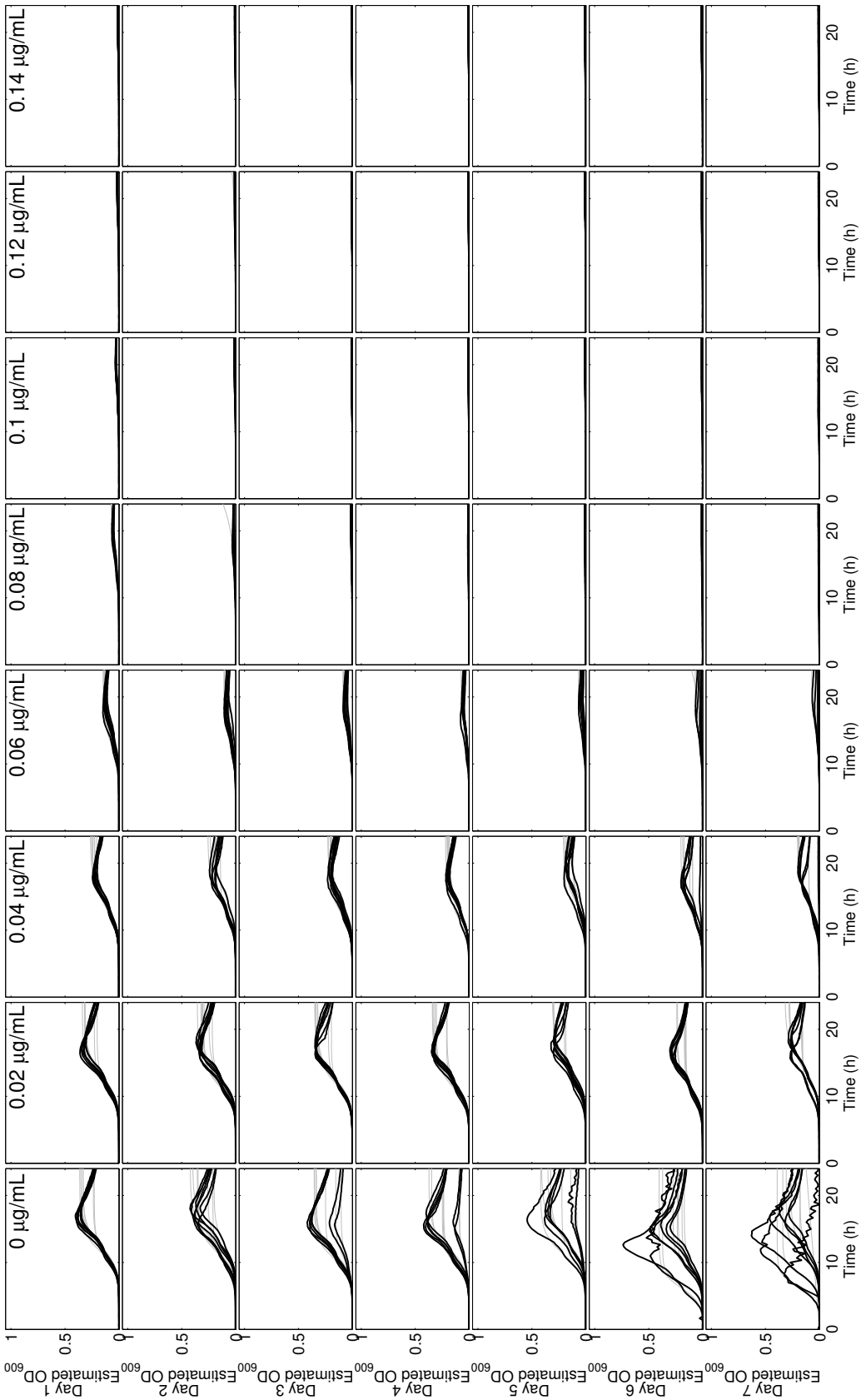

571 **Figure S4. Raw data and model fit for sensitive S strain in mixed culture conditions.** Raw optical Density data for Wyl
572 measured every 20min for seven days (black). The best fit to data (see Methods in main text) used to calculate bacterial
573 fitness is shown in grey. Each column represents one day worth of and each row the data set for one tetracycline concen-
574 tration.

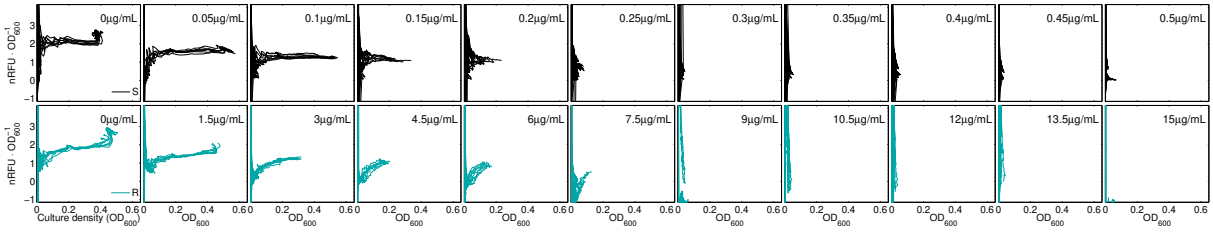

FIGURE S5. Changes in relative fluorescence over time in R and S strains in pure culture conditions. Raw change in florescence, per optical density units, measured every 20min for 24h for the S- (black) and R-type. Each column represents the data set for each tetracycline concentration used.

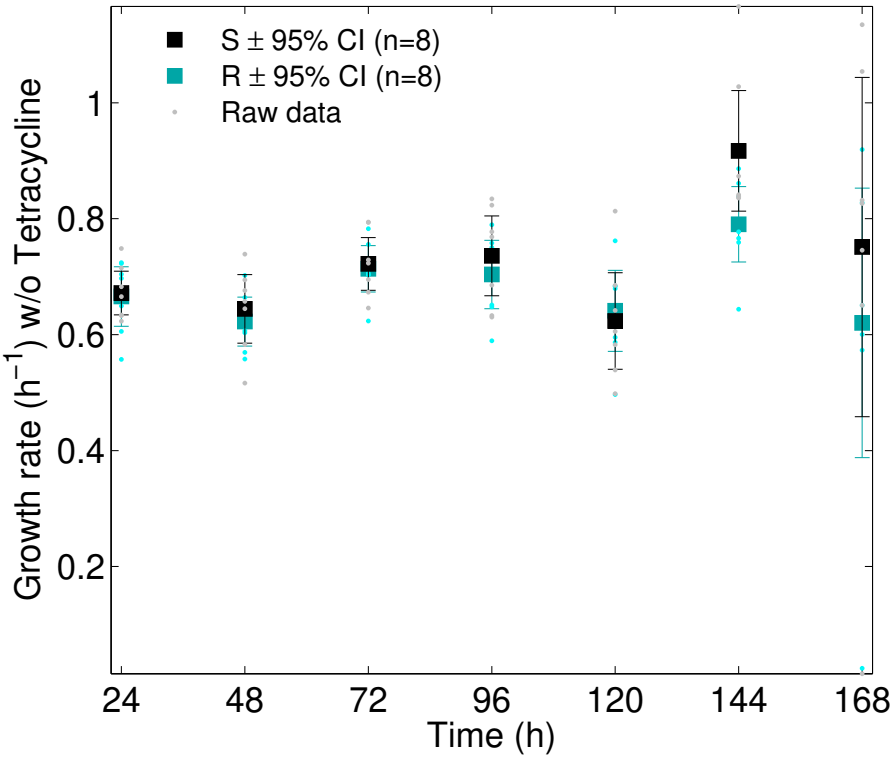

FIGURE S6. Change in growth rate over time without tetracycline. Growth rate of constructs S (black) and R (cyan) in mixed culture conditions without tetracycline. Error bars represent mean ± 95% confidence intervals, with 8 replicates. Raw data shown as dots.

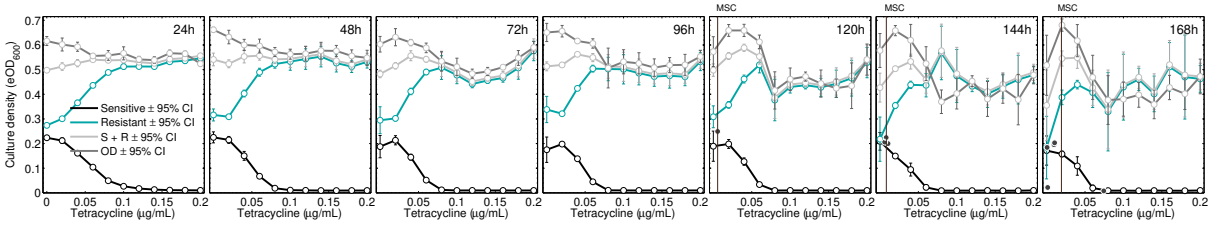

FIGURE S7. Dose-response profile for tetracycline in mixed culture conditions. Dose-response profiles for each strain (S in black, R in cyan) showing the change in culture density with increasing tetracycline concentrations over time. Error bars represent mean ± 95% confidence, with 8 replicates. Data in light grey is the optical density estimated by adding both normalised fluorescence datasets, whereas the optical density measured at 600nm is shown in dark grey. Where detectable, the minimal selective concentration is shown individually, for each replicate, as a black dot.

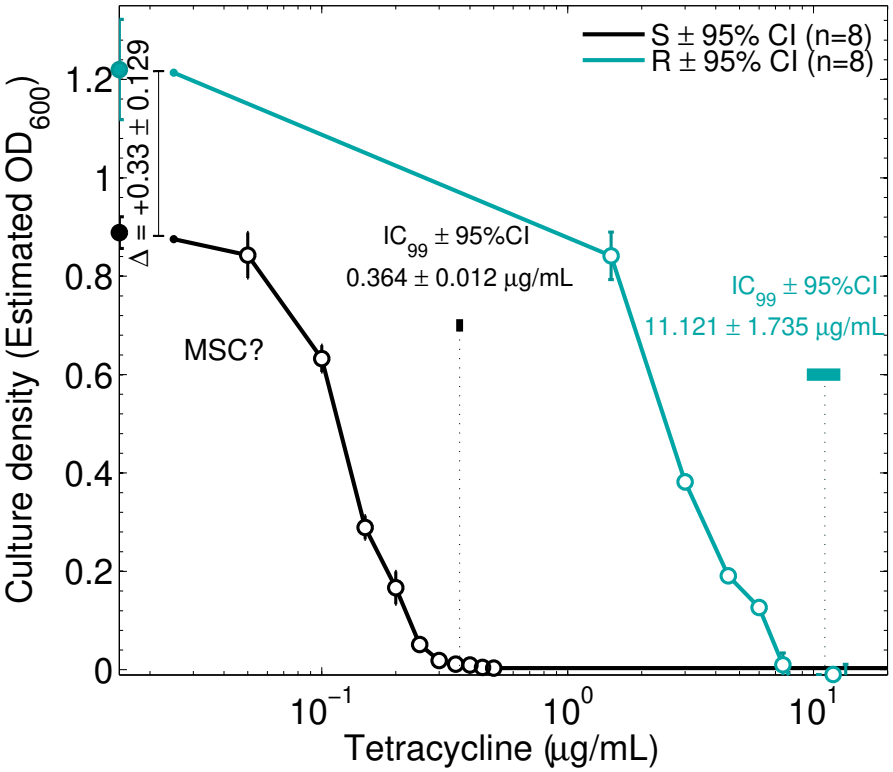

Figure S8. Dose-response profile for tetracycline (optical density data). Change in culture density for both constructs (S in black, R in cyan) in pure culture conditions, with increasing tetracycline concentrations. Error bars show mean ± 95% confidence with 8 replicates. A vertical, dashed line highlights the inhibitory concentration 99 (IC_{99}, concentration with 99% reduction in optical density with respect to the drug-free control), where the 95% confidence is noted by a horizontal line atop the IC_{99}. Note the profiles do not cross, and therefore I could not compute the minimal selective concentration or MSC. Δ shows the difference in optical density between both constructs in the absence of tetracycline (mean ± 95% confidence).

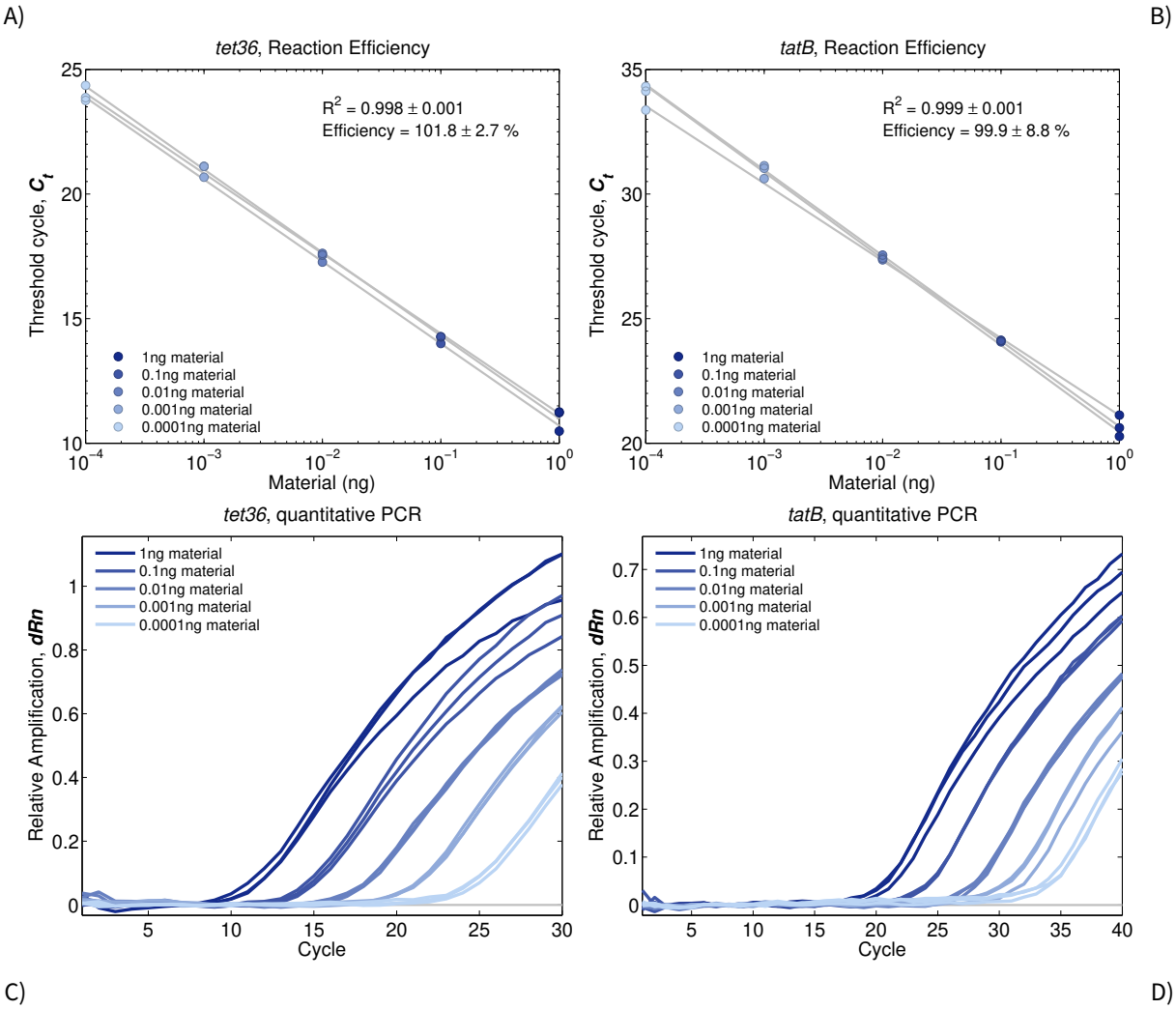

FIGURE S9. Quantitative PCR calibration curves for *tet(36)* and *tatB*. Reaction efficiency for the set of primers and probes, listed in Table 1 the main Methods section, for *tet(36)* (A) and *tatB*. The efficiency was calculated as $E_f = 10^{-1/Slope} - 1$, and the slope term calculated by fitting a linear model to qPCR threshold cycle (C_t) data. The mean ± standard deviation for the adjusted coefficient of determination R^2 and efficiency are shown in the figures. The amplification curves for each reaction, using 3 replicates, are shown in C) and D), respectively.

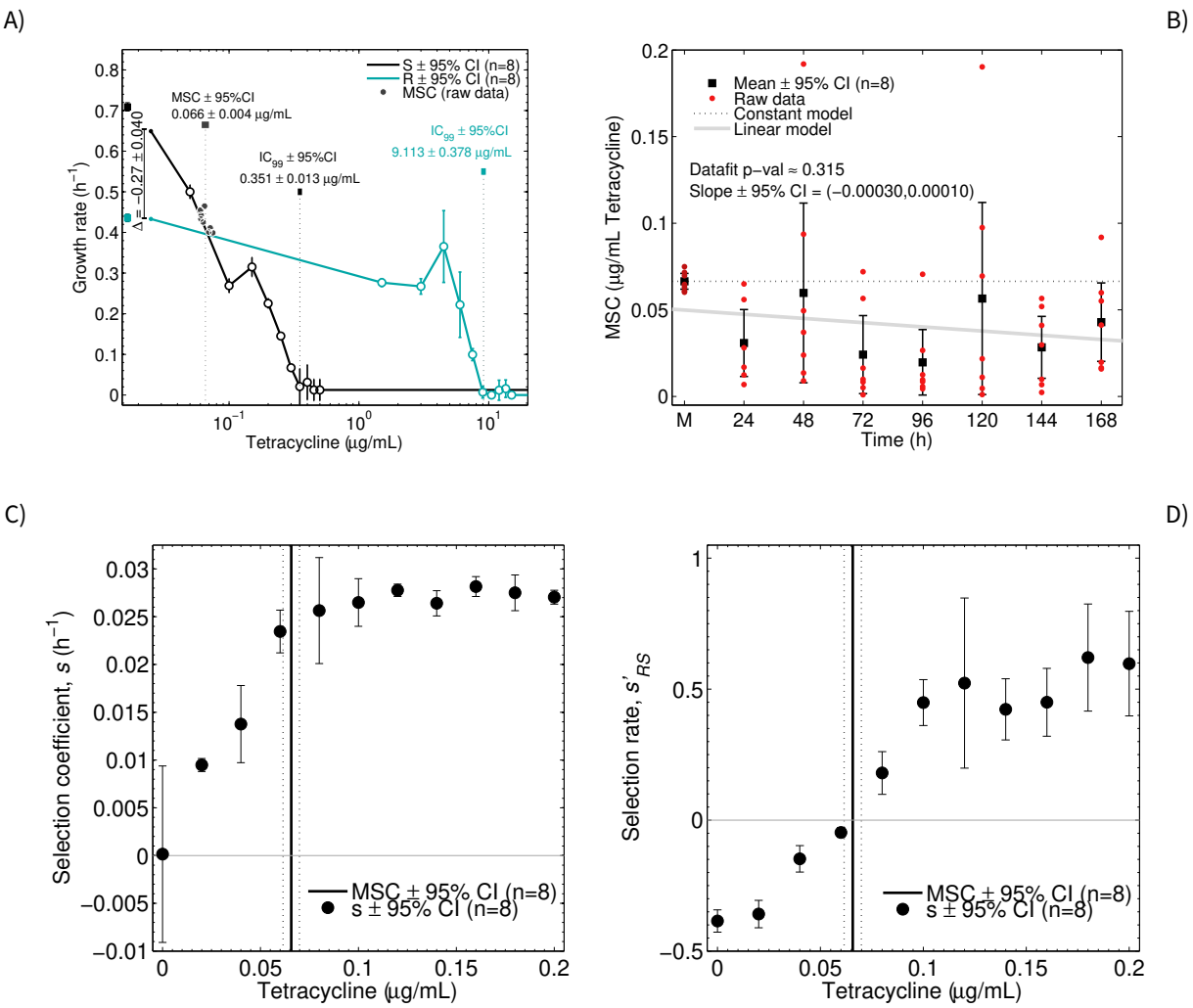

FIGURE S10. Selection of tetracycline-resistant construct R below the minimal selective concentration (MSC). A) Dose-response profile for each construct showing the change in growth rate, from fluorescence data, with increasing tetracycline concentrations. The relative difference in growth rate is noted by Δ (mean ± 95% confidence, $n = 8$). The minimal selective concentration (MSC) sat at 0.066 ± 0.004 µg/mL of tetracycline. **B)** Variation in MSC over time, with respect to that measured in monoculture (M). Error bars show mean and 95% confidence interval (8 replicates), with the raw data shown as red dots. A horizontal, dotted line represents the null hypothesis that MSC does not change through time. The grey line shows the fit of the linear model $a = bx+c$ to data where a is the MSC, b the slope with respect tetracycline concentration (x), and c the intersection with the y-axis when $x = 0$. The p value shown corresponds to an F-test on the regression model (F-statistic= 1.03) to test whether the linear model fits significantly better than a generate model consisting of only a constant term (horizontal dotted line). **C)** Selection coefficient (s) for the tetracycline-resistant construct R at different drug concentrations. The vertical black lines represent the mean (thick and black) and 95% confidence (dotted) of the MSC in A). Error bars show the mean ± 95% confidence of s at each drug concentration (8 replicates). This coefficient is measured as the ratio of construct R at the beginning ($t = 0h$) and end ($t = 168h$) of the experiment as given by the expression $s = ln[r_i(t)/r_i(0)]/t$ (see main text). **D)** Selection rate of tetracycline-resistant construct R with respect to its tetracycline-sensitive counterpart S (s_{RS}). Error bars show the selection rate for R at each tetracycline concentration (mean ± 95% confidence, 8 replicates). The vertical black lines represent the mean (thick and black) and 95% confidence (dotted) of the MSC in A). This metric is calculated using the fitness (W_{ij}) in Figure 2C, as given by the formula $s_{ij} = W_{ij} - 1$ (see main text).

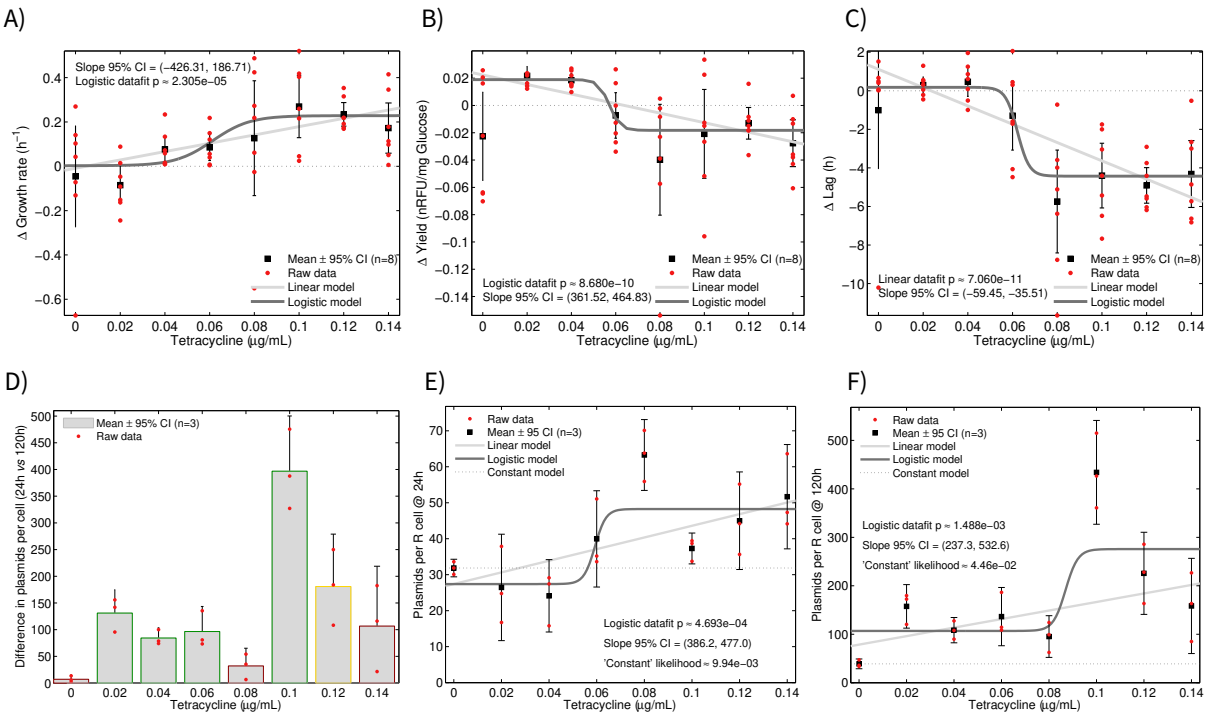

Figure S11. Variation in pGW155B copy number induces phenotypic changes in traits sensitive to plasmid carriage. A-C) Relative change in growth rate (A), biomass yield (B), and lag (C) after 168h exposure to different tetracycline concentrations. Error bars show the mean and 95% confidence interval of each trait at different drug concentrations, and raw data is shown as red dots. The horizontal, dotted black line represents the null hypothesis that no change occurs after 168h of exposure. The light grey line represents the linear model $a = bx + c$, where a notes the relative phenotypic difference, b the slope with respect tetracycline concentration (x), and c the intersect with the y-axis when $x = 0$. The dark grey line represents a 4-parameter logistic model (see main Methods). The statistics shown in A-C are those for the model with the highest adjusted coefficient of determination (R^2), where the p value shown corresponds to an F-test on the regression model to test whether it fits data significantly better than a generate model consisting of only a constant term (horizontal dotted line). **D)** Variation in pGW155B copy number after five days (120h) of exposure to tetracycline. Bars denote the mean and the errorbar 95% confidence of the mean; those with a green edge have a significant increase in copy number ($p < 0.05$) according to Welch's t-test, red if it was not ($p > 0.05$), and yellow if the test was inconclusive ($p \approx 0.05$). Raw difference in qPCR data is shown as red dots. **E-F)** Copies of pGW155B per R-cell exposed to increasing tetracycline concentrations after 24h (E) and 120h (F). Error bars note the mean and 95% confidence interval of qPCR data, and red dots raw qPCR data. The black dotted line represents the null hypothesis—no change in plasmid copy number. The predictions from linear and 4-parameter logistic models analog to those above are shown in light grey and dark grey, respectively. The statistics shown in A-C are those for the model with the highest adjusted coefficient of determination (R^2), where the p value shown corresponds to an F-test on the regression model to test whether it fits data significantly better than a generate model consisting of only a constant term (horizontal dotted line). Also shown is the relative likelihood of the null hypothesis with respect to the model (logistic or linear) with the highest adjusted coefficient of determination (R^2).

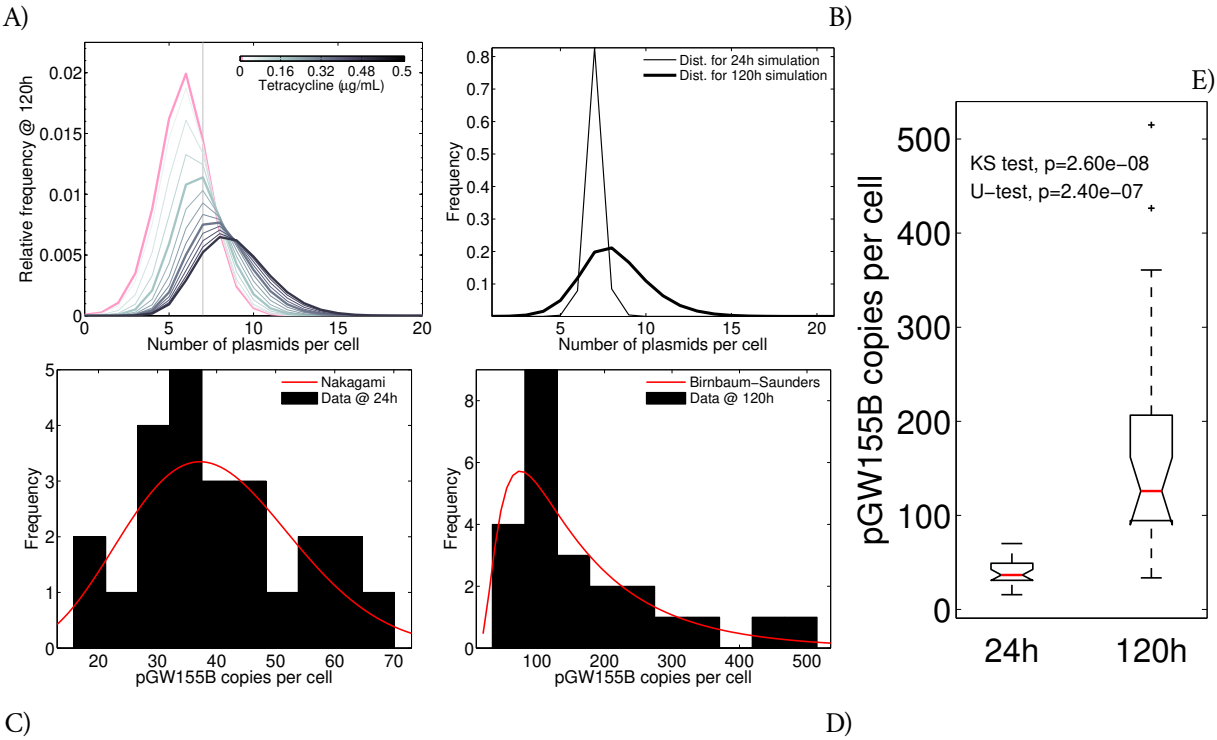

FIGURE S12. Influence of tetracycline concentration on the random segregation of pGW155B during cell division. A) Theoretical distributions of plasmid copy number as a function of antibiotic concentration. The thin, vertical line illustrates the initial distribution of plasmids—analog to the inoculum in the experimental setup. The distribution of plasmids for each drug concentration is shown in different colours from light green (low drug) to black (high drug), with thicker lines denoting higher drug concentrations. The distribution in the absence of antibiotic is shown in pink. **B)** Pooled frequency of plasmids after 24h and 120h of exposure to the drug using simulated data. **C-D)** Distribution of pGW155B copies in R-cells after 24h (C) and 120h (D) of exposure to tetracycline based on qPCR data. In red I represent the continuous distributions that best fit the data (red lines): 'Nakagami' for the 24h dataset and 'Birnbaum–Saunders' for the 120h dataset. **E)** Two-sample Kolmogorov-Smirnov (KS) and Mann–Whitney U-tests to test whether both datasets come from different distributions. The box plot shows the median (red), 75th and 25th percentile of the data set, and the whiskers extend to the most extreme data points not considered outliers. The outliers are plotted individually.